Hindawi Publishing Corporation
International Journal of Photoenergy
Volume 2014, Article ID 365862, 9 pages
http://dx.doi.org/10.1155/2014/365862

Research Article

Destruction of Toluene by the Combination of High Frequency Discharge Electrodeless Lamp and Manganese Oxide-Impregnated Granular Activated Carbon Catalyst

Jianhui Xu,[1] Chaolin Li,[1] Qian Zhang,[1,2] Di He,[3] Peng Liu,[1] and Yong Ren[1]

[1] *Environmental Science & Engineering Research Center, Harbin Institute of Technology, Shenzhen Graduate School, Shenzhen 518055, China*
[2] *Postdoctoral Innovation Practice Base, Bureau of Public Works of Longgang Shenzhen Municipality, Shenzhen, Guangdong 518172, China*
[3] *School of Civil and Environmental Engineering, University of New South Wales, Sydney, NSW 2052, Australia*

Correspondence should be addressed to Chaolin Li; lichaolinhit@gmail.com

Received 28 June 2014; Revised 21 August 2014; Accepted 8 September 2014; Published 13 October 2014

Academic Editor: Hongtao Yu

The destruction of low concentration of toluene (0–30 ppm) has been studied under the UV/photogenerated O_3/MnO_2-impregnated granular activated carbon (MnO_2-impregnated GAC) process by the combination of self-made high frequency discharge electrodeless lamp (HFDEL) with MnO_2-impregnated GAC catalyst. Experimental results showed that the initial toluene concentration can strongly affect the concentration of photogenerated O_3 from HFDEL and the efficiency and mass rate of destruction of toluene via HFDEL/MnO_2-impregnated GAC system. Active oxygen and hydroxyl radicals generated from HFDEL/MnO_2-impregnated GAC system played a key role in the decomposition of toluene process and the intermediates formed by photolysis are more prone to be mineralized by the subsequent MnO_2-impregnated GAC catalyst compared to the original toluene, resulting in synergistic mineralization of toluene by HFDEL/MnO_2-impregnated GAC system. The role of MnO_2-impregnated GAC catalyst is not only to eliminate the residual O_3 completely but also to enhance the decomposition and mineralization of toluene.

1. Introduction

Volatile organic compounds (VOCs) as widespread air pollutants can be found in both outdoor and indoor environments. The majority of VOCs originate from the exhausts of motor vehicle and solvent utilization and VOCs from the former case can react with NO_x to form tropospheric O_3 which results in smog in urban air [1]. Exposure to VOCs might cause toxic effects on central nervous system and internal organs, and the related symptoms, such as headache, respiratory tract irritation, dizziness, and nausea, are known as the sick building syndrome (SBS) [2]. For high concentration (several hundreds of ppm) of VOCs emission sources, catalytic incineration and combustion (200–900°C) have been well developed and successfully operated but are not cost-effective for low concentration of VOCs [3]. Among those available potential air-cleaning technologies for contamination of lower concentration of VOCs, photocatalytic oxidation (PCO) has caused extensive concern recently, but the problems of the poisoning or deactivation of photocatalyst caused by accumulation of organic products on the surface of catalyst have not been well solved [4, 5], which may render PCO as a technology for controlling contaminations of low concentration of VOCs inefficiently and uneconomically.

High frequency (HF) discharge electrodeless lamp (HFDEL), a typical UV light source, has been invented over 100 years and started to apply into the photolysis of organic compounds in solution and the irradiation of gases since 1970s [6]. Due to the leakage of electromagnetic radiation and ozone, however, the application of HFDEL became restricted afterwards. Unlike the conventional lamps energized by the electric field between the electrodes, the principle of HFDELs is that the gas or materials in the lamp are excited by HF

electromagnetic field to form stable UV-emitting discharge plasma. Such unique discharge pattern endows the HFDELs with lots of advantages compared to the conventional UV lamps (i.e., low pressure mercury lamps), including long lifetime of UV output, high UV/vacuum UV (VUV) radiant power, VUV-mediated generation of O_3 in conjunction with UV to create hydroxyl radicals ($HO^\bullet$), and adaptable lamp shapes. Compared to microwave discharge electrodeless lamps (MDELs), HFDELs possess higher energy conversion efficiency, have no need for resonant cavity, and overcome the short lifetime of magnetron equipped on MDELs. Employing mercury MDELs to water sterilization [7, 8] and photodissociation of organic pollutants in aqueous solution [9–12] have been studied extensively in the past few years, as mercury is the most readily to be excited, and even a domestic microwave oven may act as the microwave power supply reactor [13]. However, little has been done on the photolysis of VOCs using MDELs as the UV light source probably due to practical limitations in reactor design and operation for the treatment of gas pollutants [14]. Recently, we have investigated the photolysis of H_2S using HFDEL showing much higher removal efficiency compared to MDELs, gained some insights into the possible mechanisms for photolysis, and confirmed the feasibility of application of HFDEL into the decomposition of air pollutants [15]. To further extend the application of HFDEL, the photolysis of VOCs by HFDEL has been investigated in this study. To cope with electromagnetic radiation generated from HFDEL, stainless steel reactors have been applied in this study to minimize the negative effects of electromagnetic wave on human bodies. Meanwhile, the stainless steel reactor is also beneficial in the reflection of UV light and resistant to corrosion of corrosive gas.

Although photogenerated O_3 by HFDEL can induce advanced oxidation processes (AOPs) such as UV/O_3 to produce $HO^\bullet$ for effectively decomposing VOCs, excess O_3, as an air pollutant, in the effluent gas stream should be reduced to a safe level. Therefore, a reactor containing an O_3-decomposition catalyst (ODC) needs to be set up following the photoreactor to treat excess O_3 in the effluent gas stream. The O_3/granular activated carbon (GAC) method is relatively common in which the GAC performs dual roles: adsorption of residual O_3 and VOCs (their organic products) and decomposition of O_3 over the surface to yield $HO^\bullet$, which in turn are able to quickly mineralize VOCs and their organic products adsorbed on the surface of GAC and/or in gas phase [16]. To further enhance the O_3 decomposition and generation of $HO^\bullet$ for mineralization of VOCs and their organic products, the impregnation of MnO_2 on GAC has been applied in this study as MnO_2 shows an excellent simultaneous elimination of VOCs and O_3 [17]. In addition to the elimination of excess O_3 and enhanced removal of VOCs, the combination of HFDEL and ODC may also have the following advantages: (i) the photolysis of VOCs results in the partial mineralization of VOCs, which may reduce the accumulation of organic intermediates on the surface of ODC and extend the lifetime of ODC, (ii) photogenerated O_3 may have a positive effect on the regeneration of ODC considering that O_3 photogenerated from HFEDL can regenerate the photocatalyst [18], and (iii) the organic intermediates of photolysis may be more subject to be mineralized by MnO_2-impregnated/O_3 compared to the original VOCs.

In this study, a preliminary study on the removal of VOCs with the combination of HFDEL and MnO_2-impregnated GAC was investigated. Filled with binary mixtures of Hg-Ar, HFDEL was found to emit intense atomic lines of mercury in both UV and VUV region (mainly atomic Hg emission lines at 185 nm ($6s6p(^1P_1)$–$6s6p(^1S_0)$) and 253.7 nm (6^2P_1–6^2S_0) [15] and MnO_2-impregnated GAC was confirmed to decompose O_3 and induce the formation of $O^\bullet$ and $HO^\bullet$ following the exposure to O_3. A relatively low concentration level of toluene as the target VOC, in the range of 0–30 ppm, was selected for this work, in the consideration of ubiquitousness of indoor and outdoor environments. The performances of removal and mineralization of toluene were examined under different conditions with photolysis by HFDEL, MnO_2-impregnated GAC-mediated catalyzed ozonation, and the combination of HFDEL and MnO_2-impregnated GAC. The analysis of intermediates and possible mechanisms for photolysis and catalyzed ozonation were also evaluated in this study.

2. Materials and Methods

2.1. HFDEL. HFDEL consisted of an HF power supply and electrodeless lamps. The HF power supply was operated to produce a current with a fixed frequency of 2.45 MHz, which was transmitted to a coupling fixture to generate an HF electromagnetic field. The mercury atoms were excited by the HF electromagnetic field followed by returning to ground state to emit UV light [13, 19]. The working power for HFDEL was 80 W which was sufficient to ignite the quartz lamp. The electrodeless lamps were made of quartz bulb with the height of 15 cm (the volume is ~550 mL).

2.2. Characterization of HFDEL. The emission spectrum of UV radiation emitted by HFDEL was detected by an Acton VM-505 VUV monochromator. The stability of light intensity of HFDEL at 253.7 nm was monitored at the outflow of the photolysis reactor by an irradiatometer (TN-2254, Taiwan Taina Instrument) while the distribution of light intensity at 253.7 nm as a function of the distance to the bottom center of the lamp was measured by the same irradiatometer. More details have been shown in Supplementary Material available online at http://dx.doi.org/10.1155/2014/365862 (SM) (Figures SM1–3).

2.3. MnO_2-Impregnated GAC. Wood-based GAC (cylinder shape with a diameter of 4 cm) was selected as supporting material in this study (Calgon Carbon Corporation in Tianjin, China). Firstly, GAC was acid-treated in a 5% solution of hydrochloric acid for 6 h to reduce ash content, washed with Milli-Q water (MQ) repeatedly to reach neutrality, and dried at 105°C for 24 h. Then 500 g GAC and certain amounts of $Mn(NO_3)_2$ were mixed with 2 L MQ and constantly shaken for 24 hours at 25°C for the preparation of MnO_2-impregnated GAC with different mass loading of MnO_2 from 0 to 10%. The concentration of Mn^{2+}

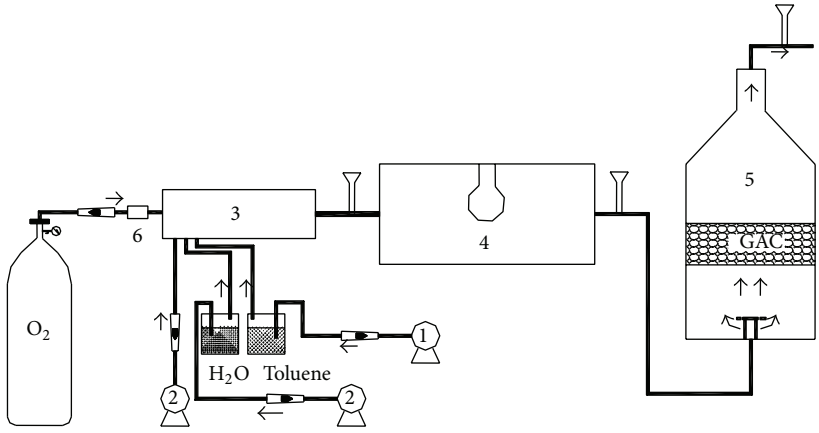

(1) Continuous flow toluene gas generation system
(2) Experimental parameter control system
(3) Mixing tube
(4) HFDEL
(5) MnO_2-impregnated GAC system
(6) Ozone generator

Figure 1: The sketch of experimental setup of the combination of HFDEL with MnO_2-impregnated GAC system.

in the supernatant was characterized by inductively coupled plasma-optical emission spectrometry (ICP-OES) (Varian AX, Varian) confirming ~100% Mn^{2+} has been adsorbed on GAC. Afterwards, the solids were filtrated and dried overnight at 105°C for 12 h in an air oven and calcinated at 450°C in muffle furnace for 6 h. Mineralogy of the MnO_2 was characterized by X-ray diffraction (Rigaku D/MAX 2500). The surface morphology of MnO_2-impregnated GAC was obtained by scanning electron microscope (Hitachi S-4700).

2.4. Experimental Setup. The experimental setup designed for the evaluation of toluene removal efficiency by HFDEL/MnO_2-impregnated GAC is shown in Figure 1. The system consisted of an experimental parameter control system, a continuous flow gas generation system, HFDEL stainless steel reactor, and MnO_2-impregnated GAC system. The toluene gas was pumped via the bubbling of air into the toluene solution (1) and the humidity was adjusted to 74.1% through the experimental parameter control system (2). The mixture of toluene was transferred through a mixing tube (3) before introducing into the photolysis area (4), which is followed by MnO_2-impregnated GAC system (5). The ozone generator (6) was only applied to investigate the effect of O_3/MnO_2-impregnated GAC on the removal of toluene. The gas stream passed through the reactor for 15 min to allow the system to reach the steady state. Power was then applied to inspire the lamp for another 10 min to make sure the steady state of light intensity had been achieved before the measurement of concentration of toluene in the gas stream. The initial toluene concentration ranged from 0 to 30 ppm. All the experiments were carried out at fixed gas flow rate of 4 $m^3\,h^{-1}$ at room temperature (25 ± 2°C).

2.5. Chemical Analysis. The concentration of toluene and its final product CO_2 in the air stream was analyzed by a gas chromatograph (GC, Thermo Finnigan) equipped with flame ionization detector (FID), respectively. The concentration of O_3 was monitored spectrophotometrically at 254 nm where O_3 possesses a molar absorptivity of 3292 ± 70 $M^{-1}\,cm^{-1}$ [20]. The gaseous intermediates in the outlet gas were collected by an absorption bottle filled with HPLC grade methanol (Dima Technology, USA) for 1 h after the reaction reached equilibrium. The solution was analyzed by GC (Agilent 6890A)-MSD (Agilent 5975C with Triple-Axis Detector). The carrier gas was ultrahigh purity helium at a constant flow rate of 1 mL min^{-1}. The injector and detector temperatures were set at 230 and 270°C, respectively. The GC column was DB-5 (30 m × 0.25 mm × 0.25 mm, Agilent technology). The temperature of the GC oven was initially set at 80°C for 1 min and then raised at 5°C min^{-1} to 250°C for 3 min with a subsequent increase to a final 300°C at a rate of 10°C min^{-1} for 5 min. 1.0 μL of sample was injected in the splitless mode.

3. Results

3.1. Generation of O_3. As photogenerated O_3 can induce AOPs including UV/O_3 and MnO_2-impregnated GAC/O_3 to create $HO^\bullet$ for effective decomposition of toluene, the concentration of generated O_3 as a function of inlet toluene concentration was investigated. Figure 2 shows that the concentration of photogenerated O_3 decreased from 130 to 41 ppm with an increase in the inlet toluene concentration from 0 to 30 ppm. The possible pathway of O_3 formation during the UV photolysis process is as follows (see (1)–(3)):

$$O_2 + h\nu \ (\lambda < 200\,\text{nm}) \longrightarrow O^\bullet + O^\bullet \quad (1)$$

$$H_2O + O^\bullet \longrightarrow HO^\bullet + HO^\bullet \quad (2)$$

$$O_2 + O^\bullet \longrightarrow O_3 \quad (3)$$

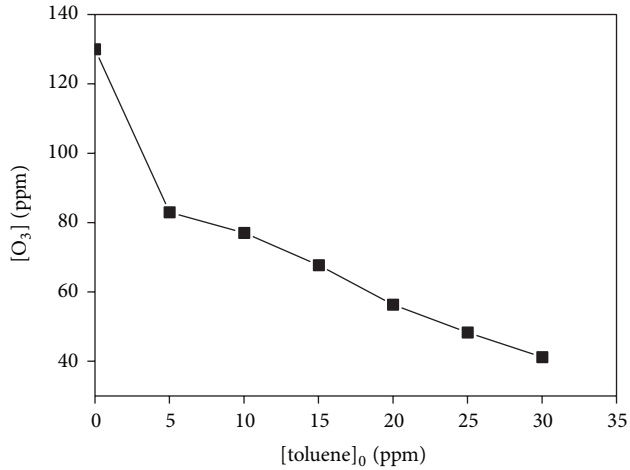

Figure 2: Photogenerated O_3 concentration as a function of inlet toluene concentration.

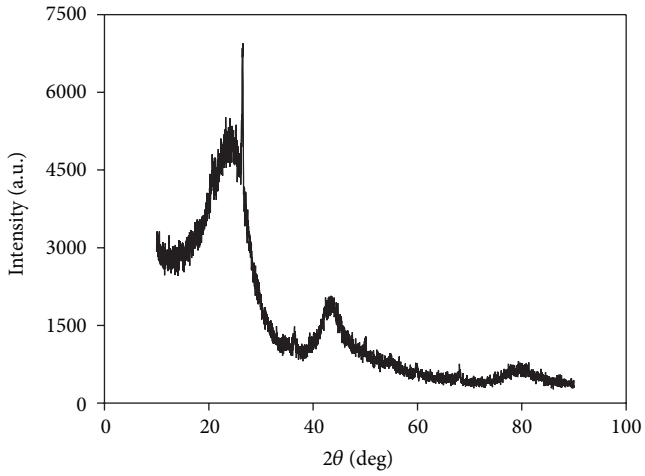

Figure 3: XRD pattern of MnO_2-impregnated GAC.

$O^\bullet$ is commonly regarded as the main oxidant in the catalytic ozonation [21]. The primary pathway of toluene oxidation by $O^\bullet$ is the abstraction of hydrogen atoms from the methyl group, directly resulting in the production of benzyl alcohol or/and benzaldehyde, which were further attacked by an $O^\bullet$ leading to benzoic acid or the direct opening of the aromatic ring followed by mineralization of intermediates by $O^\bullet$ [22]. With an increase in the inlet concentration of toluene, therefore, the consumption of $O^\bullet$ by toluene increases, which may result in a decrease in the generation of O_3 during photolysis process (see (3)).

3.2. Optimization of MnO_2-Impregnated GAC. In addition to the elimination of excess O_3, MnO_2-impregnated GAC was also applied to enhance the removal of toluene through the catalyzed-ozonation process. The XRD pattern of MnO_2-impregnated GAC is shown in Figure 3. Besides two basic diffraction peaks ($2\theta = 24^\circ$ and 43°), there is a sharp and intense peak at about $2\theta = 26^\circ$, which is identified with the typical spectrum of β-MnO_2 phase [23], the most stable

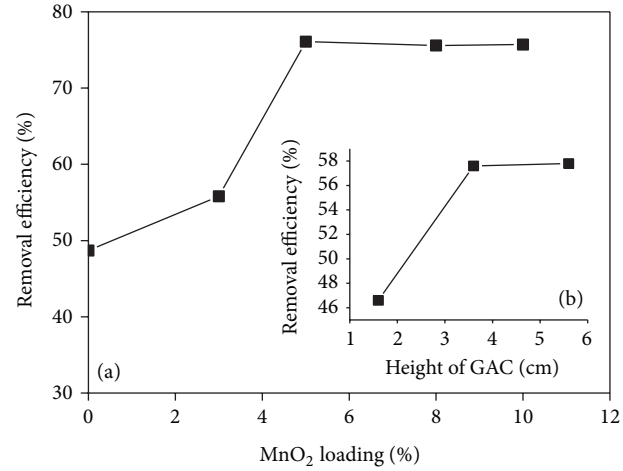

Figure 4: Removal efficiency of toluene as a function of (a) MnO_2 loading and (b) height of GAC during the O_3/MnO_2-impregnated GAC process. Experimental conditions: (a) $[O_3]_0$ = 40 ppm; $[toluene]_0$ = 9 ppm; the height of GAC = 1.6 cm; (b) $[O_3]_0$ = 40 ppm; $[toluene]_0$ = 20 ppm; the loading of MnO_2 = 5%.

structure in a variety of Mn (IV) oxides structural forms at low temperatures [23]. In addition, significant instrumental noises indicate that MnO_2 impregnated on the surface is amorphous in structure. Figure 4(a) shows the removal efficiency of toluene as a function of the loading of MnO_2 impregnated on GAC (0–10%), where the inlet concentrations of toluene and O_3 are 9 and 40 ppm, respectively, and the depth of GAC is fixed at 1.6 cm. To evaluate the "real" decomposition of toluene by MnO_2-impregnated GAC/O_3, all adsorption sites of MnO_2-impregnated GAC were saturated with toluene followed by the introduction of O_3 (the breakthrough curve for the adsorption of toluene by MnO_2-impregnated GAC has been shown as in Figure SM-4). Since it has been confirmed previously that molecular O_3 reacts very slowly with toluene ($1.4\,M^{-1}\,s^{-1}$) [24], the observed reduction of toluene by MnO_2-impregnated GAC/O_3 in Figure 4 could be largely the result of a partial formation of $HO^\bullet$ and $O^\bullet$ (the rate constants for the reaction of toluene with $HO^\bullet$ and $O^\bullet$ are 3.0×10^9 [25] and $2.1 \times 10^9\,M^{-1}\,s^{-1}$ [26], resp.), which is consistent with other reports that the decomposition of toluene and its intermediates mainly result from the presence of $HO^\bullet$ and $O^\bullet$ produced during O_3 decomposition over MnO_2 layer [17, 27, 28]. With an increase in the loading of MnO_2 from 0 to 5%, the impregnation of MnO_2 on GAC indeed enhanced the decomposition of toluene from 49 to 76% while the degradation of toluene remained unchanged (76%) with a further increase in the loading of MnO_2 from 5 to 10%, which could be attributed to (i) the complete consumption of O_3 which halts the initiation of $HO^\bullet$ and $O^\bullet$ formation and/or (ii) overloading of MnO_2 which could block the access of O_3 to surface sites within the pores of GAC, as shown in Figure 5. Therefore, the optimal loading of MnO_2 is selected as 5% when the inlet concentration of O_3 is 40 ppm.

Similarly, the effect of depth of GAC layer on the decomposition of toluene was also investigated. The MnO_2- (5%)

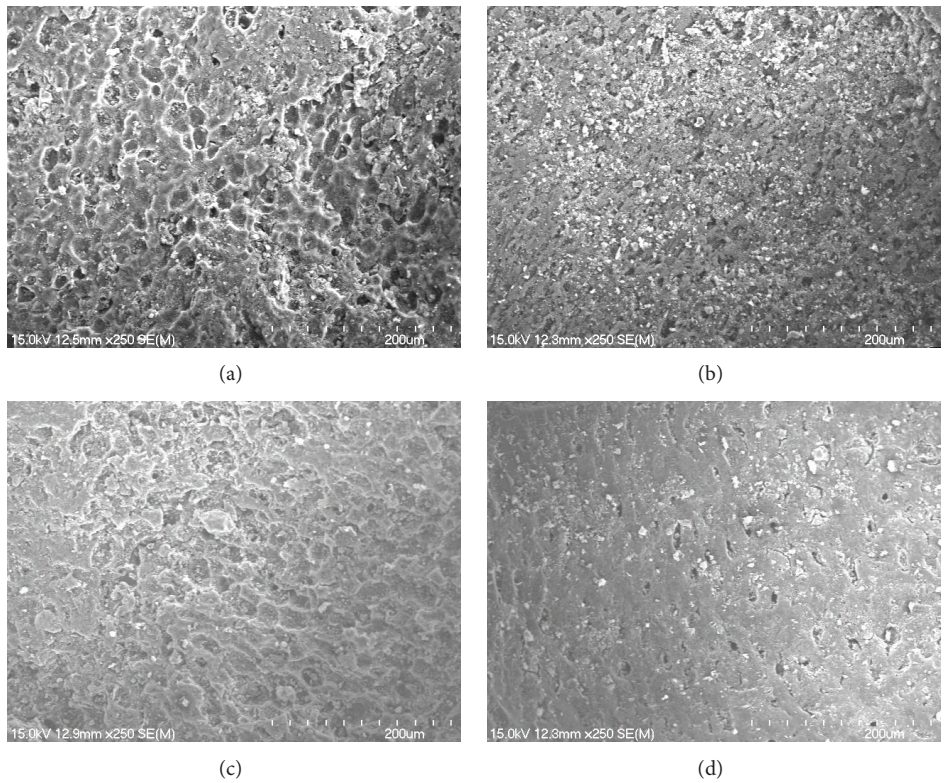

Figure 5: SEM images of MnO_2-impregnated GAC with the different loading of MnO_2 (a) 0%; (b) 3%; (c) 5%; (d) 10%.

impregnated GACs with different layer depths were saturated with toluene followed by the introduction of 40 ppm O_3 and 20 ppm toluene, respectively. Figure 4(b) demonstrates that, with an increase in the depth of GAC layer from 1.6 to 3.6 cm, the decomposition of toluene increased from 47 to 58% while a further increase in the depth of GAC layer from 3.6 to 5.6 cm did not result in a further removal of toluene, which could be attributed to the complete elimination of O_3 by MnO_2-impregnated GACs. As the photogenerated O_3 increased from 41 to 130 ppm with a decrease in the inlet toluene concentration from 30 to 0 ppm, the ODC system filled with MnO_2-impregnated GACs must be capable of removing 130 ppm O_3 completely. No detection of O_3 in the effluent gas stream has been confirmed when the loading of MnO_2 is 5% and the depth of GAC layer is 3.6 cm. As the inlet O_3 concentration varies with the initial concentration of toluene, it might be unrealistic to optimize the loading of MnO_2 and depth of GAC for each concentration of toluene. For consistency, therefore, the loading of MnO_2 and the depth of GAC layer were selected as 5% and 4.0 cm in the following experiments, respectively.

3.3. Decomposition and Mineralization of Toluene. Figures 6(a) and 7(a) show the removal and mineralization efficiency of toluene as a function of inlet toluene concentration from 5 to 30 ppm, respectively. The efficiencies of toluene decomposition by HFDEL, MnO_2-impregnated GAC/O_3, and HFDEL/MnO_2-impregnated GAC were observed (Figure 6(a)) to decrease from 90 to 46%, 94 to 30%, and 100 to 55%, respectively, while the efficiencies of toluene mineralization by HFDEL, MnO_2-impregnated GAC/O_3, and HFDEL/MnO_2-impregnated GAC (Figure 7(a)) decreased from 74 to 12%, 86 to 7%, and 100 to 23%, respectively, as the inlet toluene concentration increases from 5 to 30 ppm. It is noted that the inlet O_3 concentration in the case of MnO_2-impregnated GAC/O_3 is consistent with the concentration of photogenerated O_3 from HFDEL as a function of inlet toluene concentration. Since the number and energy of photons and active radicals in the reaction area did not change at a fixed input HF power and a constant dosage of catalyst, with constant gas flow rate, unit toluene obtains less energy as inlet toluene concentration increases, which results in relatively lower removal and mineralization efficiencies of higher concentration of inlet toluene. The HFDEL/MnO_2-impregnated GAC possesses higher removal efficiency compared to HFDEL only, which implies the combination of HFDEL with MnO_2-impregnated GAC indeed enhances the removal of toluene. More importantly, the synergistic effects of the mineralization of toluene by HFDEL/MnO_2-impregnated GAC were found in Figure 7(a) in which the mineralization efficiency of toluene by HFDEL/MnO_2-impregnated GAC is higher than the summation of the efficiency by HFDEL only and MnO_2-impregnated GAC/O_3 under the circumstances of the inlet toluene concentration between 20 and 30 ppm, suggesting the photolysis of toluene by HFDEL enhances the subsequent mineralization of toluene by MnO_2-impregnated GAC/O_3. These synergistic effects could be attributed to

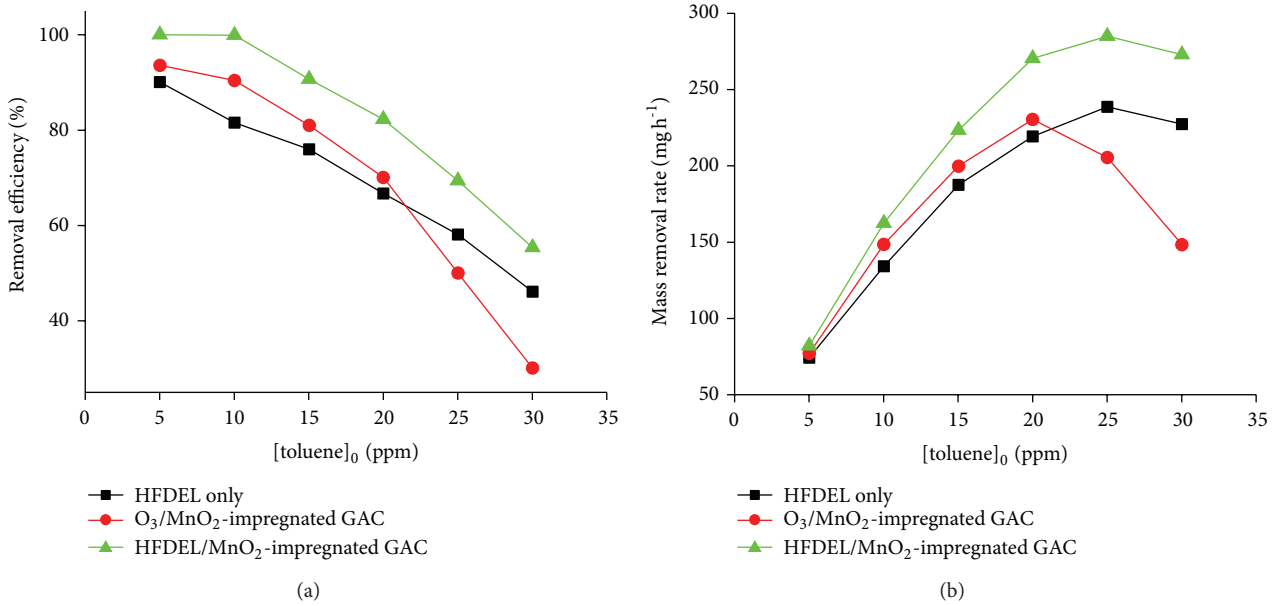

FIGURE 6: (a) Removal efficiency and (b) mass removal rate of toluene as a function of inlet toluene concentration by HFDEL only, O_3/MnO_2-impregnated GAC, and HFDEL/MnO_2-impregnated GAC, respectively. Note that the inlet O_3 concentration in O_3/MnO_2-impregnated GAC is consistent with the photogenerated O_3 from HFDEL.

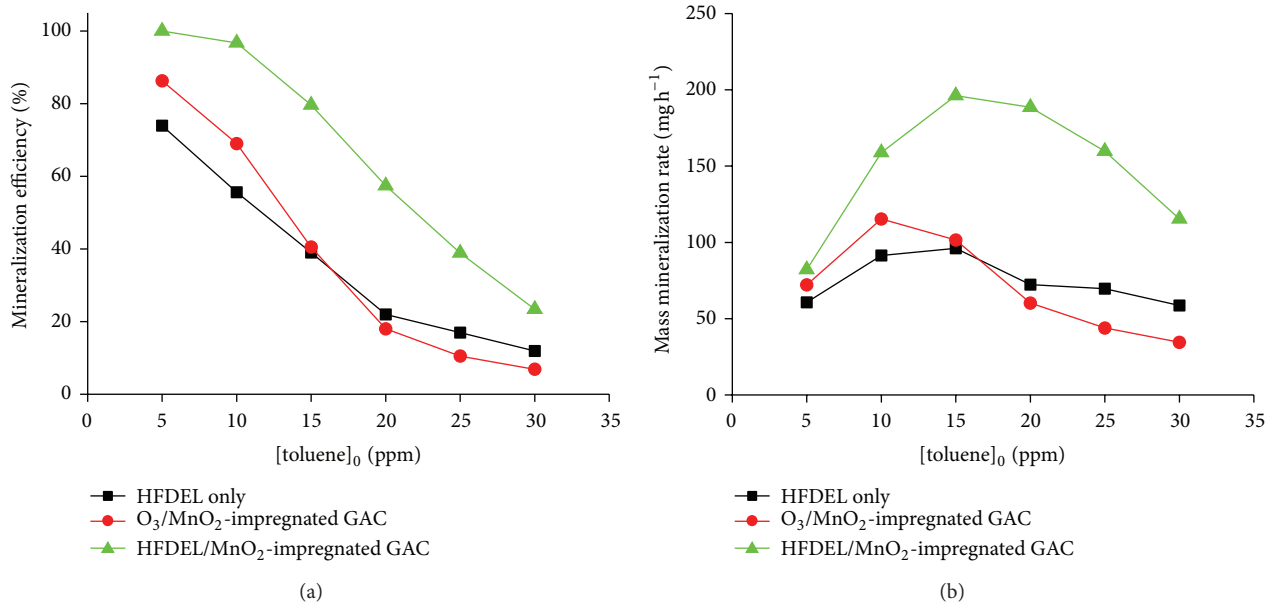

FIGURE 7: (a) Mineralization efficiency and (b) mass mineralization rate of toluene as a function of inlet toluene concentration by HFDEL only, O_3/MnO_2-impregnated GAC, and HFDEL/MnO_2-impregnated GAC, respectively. Note that the inlet O_3 concentration in O_3/MnO_2-impregnated GAC is consistent with the photogenerated O_3 from HFDEL.

the formation of intermediates during the photolysis process which are subjected to be mineralized by $HO^\bullet$ and $O^\bullet$ formed during O_3 decomposition over MnO_2-impregnated GAC compared to the original toluene [22].

Figures 6(b) and 7(b) demonstrate the removal and mineralization mass rate of toluene as a function of inlet toluene concentration from 5 to 30 ppm, respectively. The mass rates of toluene decomposition and mineralization by HFDEL, MnO_2-impregnated GAC/O_3, and HFDEL/MnO_2-impregnated GAC followed a similar profile which increased initially followed by a decrease with an increase in the inlet toluene (Figures 5(b) and 6(b)). During the photolysis process, $O^\bullet$ and $HO^\bullet$ formed via the absorbance of $h\nu$ ($\lambda <$ 200 nm) by O_2 and H_2O, respectively (see (1) and (2)), are sufficient for low concentration of inlet toluene and thus the removal and mineralization mass rate increases with the inlet

toluene concentration. With the inlet toluene concentration approaching to a certain concentration, however, toluene starts to compete with O_2 and H_2O to consume UV light at 185 nm, resulting in a lower production rate of $O^\bullet$ and $HO^\bullet$. Although the direct photolysis of toluene by UV light at 185 nm can occur, the conversion rate of toluene by direct photolysis is much lower than that by $O^\bullet$ and $HO^\bullet$, respectively [17], thus resulting in a decrease in the removal and mineralization mass rate with a further increase in the inlet toluene concentration. For the catalyzed ozonation process (MnO_2-impregnated GAC/O_3), a decrease in the removal and mineralization mass rate of toluene with a further increase in the inlet toluene concentration was due to the decrease in the inlet O_3 concentration with increasing in the inlet toluene concentration as the inlet O_3 concentration in this study needs to be consistent with the photogenerated O_3 concentration (Figure 2). For the low concentration of inlet toluene, an increase in removal and mineralization mass rate with the inlet toluene concentration can be observed since the high concentration of inlet O_3 combined with MnO_2-impregnated GAC results in the sufficient amount of $O^\bullet$ and $HO^\bullet$ for decomposition of toluene.

4. Discussion

In this study, we have shown that the removal efficiency of toluene using HFDEL depends on the inlet toluene concentration and the combination of MnO_2-impregnated GAC with HFDEL can not only eliminate the residual O_3 but also enhance the removal of toluene. More importantly, the synergistic effects of HFDEL/MnO_2-impregnated GAC on the mineralization of toluene have also been confirmed, showing the intermediates formed during the photolysis process are prone to be mineralized by the following MnO_2-impregnated GAC catalyzed ozonation process. Possible mechanisms for the removal of toluene by UV/O_3/MnO_2-impregnated GAC will be discussed in this section.

Under oxygen environment, the photo energy of VUV light at 185 nm produced by HFDEL is capable of destroying the bond of O=O (491 kJ mol^{-1}), resulting in formation of $O^\bullet$ (see (1)) with a subsequent generation of $HO^\bullet$ and O_3 (see (2) and (3)) [29, 30]. Photogenerated O_3 can efficiently be decomposed into $O^\bullet$ by UV irradiation (see (4)) and $O^\bullet$ can further react with H_2O and O_3 to generate $HO^\bullet$, respectively (see (2) and (5)) [31, 32]:

$$O_3 + h\nu \ (\lambda < 254\,\text{nm}) \longrightarrow O^\bullet + O_2 \quad (4)$$

$$H_2O + O_3 \longrightarrow 2HO^\bullet + O_2 \quad (5)$$

For O_3 decomposition over the layer of MnO_2-impregnated GAC, O_3 can be also decomposed to form $O^\bullet$ on the active sites of MnO_2-impregnated GAC surface (see (6)) and $O^\bullet$ can further react with H_2O and O_3 to generate $HO^\bullet$, respectively (see (2) and (5)) [17]:

$$O_3 + * \longrightarrow O^\bullet + O_2 \quad (6)$$

where * represents active sites on MnO_2-impregnated GAC surface. Due to the limited direct photolysis of toluene by VUV at 185 nm, the primary pathway of toluene oxidation was the H-abstraction from the methyl group by $HO^\bullet$ and $O^\bullet$, resulting in two pathways of toluene destruction in the UV/O_3/MnO_2-impregnated GAC process.

The primary pathway of toluene oxidation by $HO^\bullet/O^\bullet$ was the H-abstraction from the methyl group, resulting in the production of a benzyl radical and then the formation of benzyl alcohol and/or benzaldehyde [22], which were further attacked by $HO^\bullet/O^\bullet$ leading to benzoic acid followed by the opening of the aromatic ring [33–35]. The compounds generated after the ring opening were substances with low molecular mass, such as formic acid, acetic acid, and CO, with a subsequent formation of harmless CO_2 and H_2O by the attack of $HO^\bullet/O^\bullet$. In our study, benzyl alcohol and benzaldehyde dimethyl acetal (BDA) as intermediates were detected by GC-MS analysis (Figure SM5). The presence of BDA, the product of aldol condensation of benzaldehyde and methanol under acidic conditions, suggests that benzaldehyde is formed during the photolysis of toluene. Due to the lack of detection of benzoic acid, the acidic environment for the formation of BDA could be attributed to the formation of low molecular-weight acid (e.g., formic acid and acetic acid). The low boiling point of these small organic acids leads to no direct evidence to confirm their presence by GC-MS. In summary, it can be proposed that the intermediates including benzyl alcohol and benzaldehyde are produced from the HFDEL system followed by the direct opening of the aromatic ring without formation of benzoic acid by the attack of $HO^\bullet/O^\bullet$. Compared to the original toluene compounds, these intermediates are more subjected to be decomposed to small molecules followed by the formation of CO_2 and H_2O via the subsequent O_3/MnO_2-impregnated GAC process, resulting in the synergistic mineralization of toluene using the HFDEL/MnO_2-impregnated GAC process.

5. Conclusion

The destruction of low concentration of toluene (0–30 ppm) has been studied under the advanced photooxidation processes by the combination of self-made HFDEL with MnO_2-impregnated GAC catalyst. The conclusions are as follow:

(1) The concentration of photogenerated O_3 from HFDEL decreased from 130 to 41 ppm with an increase in the inlet toluene concentration from 0 to 30 ppm.

(2) The efficiency of decomposition of toluene by HFDEL decreased from 90 to 46% as the inlet toluene concentration increases from 5 to 30 ppm. The introduction of MnO_2-impregnated GAC catalyst is not only to eliminate the residual O_3 (41–130 ppm) completely but also to enhance the decomposition of toluene by ~10%. (The mass loading of MnO_2 and the depth of GAC layer were 5% and 4.0 cm, resp.)

(3) Active oxygen and hydroxyl radicals generated from HFDEL/MnO_2-impregnated GAC system played a key role in the decomposition of toluene process. The intermediates formed by photolysis are more

prone to be mineralized by the subsequent MnO_2-impregnated GAC catalyst compared to the original toluene, resulting in synergistic mineralization of toluene by HFDEL/MnO_2-impregnated GAC system.

In summary, the combination of HFDEL and MnO_2-impregnated GAC efficiently enhances the toluene destruction process, eliminates the residual O_3, and, more importantly, fulfills the synergistic mineralization of toluene, demonstrating that HFDEL/MnO_2-impregnated GAC system will be a promising air-cleaning technology for contamination of lower concentration of VOCs.

Conflict of Interests

The authors declare that there is no conflict of interests regarding the publication of this paper.

Acknowledgments

This work was supported by the National Natural Science Foundation of China (Grant no. 51178135) and China Postdoctoral Science Foundation (Grant no. 2014M560267).

References

[1] L. Zou, Y. Luo, M. Hooper, and E. Hu, "Removal of VOCs by photocatalysis process using adsorption enhanced TiO_2-SiO_2 catalyst," *Chemical Engineering and Processing: Process Intensification*, vol. 45, no. 11, pp. 959–964, 2006.

[2] Y. M. Kim, S. Harrad, and R. M. Harrison, "Concentrations and sources of VOCs in urban domestic and public microenvironments," *Environmental Science and Technology*, vol. 35, no. 6, pp. 997–1004, 2001.

[3] J. Peral, X. Domenech, and D. F. Ollis, "Heterogeneous photocatalysis for purification, decontamination and deodorization of air," *Journal of Chemical Technology and Biotechnology*, vol. 70, pp. 117–140, 1997.

[4] T. X. Liu, X. Z. Li, and F. B. Li, "$AgNO_3$-induced photocatalytic degradation of odorous methyl mercaptan in gaseous phase: Mechanism of chemisorption and photocatalytic reaction," *Environmental Science and Technology*, vol. 42, no. 12, pp. 4540–4545, 2008.

[5] T.-X. Liu, F.-B. Li, and X.-Z. Li, "Effects of peptizing conditions on nanometer properties and photocatalytic activity of TiO_2 hydrosols prepared by H_2TiO_3," *Journal of Hazardous Materials*, vol. 155, no. 1-2, pp. 90–99, 2008.

[6] I. E. Den Besten and J. W. Tracy, "Electrodelessly discharged photochemical lamps," *Journal of Chemical Education*, vol. 50, no. 4, p. 303, 1973.

[7] S. Iwaguch, K. Matsumura, Y. Tokuoka, S. Wakui, and N. Kawashima, "Sterilization system using microwave and UV light," *Colloids and Surfaces B: Biointerfaces*, vol. 25, no. 4, pp. 299–304, 2002.

[8] I. Pandithas, K. Brown, A. I. Al-Shamma'a, J. Lucas, and J. J. Lowke, "Biological applications of a low pressure microwave plasma UV lamp," in *Proceedings of the 14th IEEE International Pulsed Power Conference (Ppc '03)*, vol. 1-2, pp. 1112–1115, 2003.

[9] S. Horikoshi, H. Hidaka, and N. Serpone, "Environmental remediation by an integrated microwave/UV-illumination method, 1. Microwave-assisted degradation of rhodamine-B dye in aqueous TiO_2 dispersions," *Environmental Science and Technology*, vol. 36, no. 6, pp. 1357–1366, 2002.

[10] S. Horikoshi, H. Hidaka, and N. Serpone, "Environmental remediation by an integrated microwave/UV illumination technique. 3. A microwave-powered plasma light source and photoreactor to degrade pollutants in aqueous dispersions of TiO_2 illuminated by the emitted UV/visible radiation," *Environmental Science and Technology*, vol. 36, no. 23, pp. 5229–5237, 2002.

[11] S. Horikoshi, H. Hidaka, and N. Serpone, "Environmental remediation by an integrated microwave/UV illumination technique VI. A simple modified domestic microwave oven integrating an electrodeless UV-Vis lamp to photodegrade environmental pollutants in aqueous media," *Journal of Photochemistry and Photobiology A*, vol. 161, no. 2-3, pp. 221–225, 2004.

[12] S. Horikoshi, F. Hojo, H. Hidaka, and N. Serpone, "Environmental remediation by an integrated microwave/UV illumination technique. 8. Fate of carboxylic acids, aldehydes, alkoxycarbonyl and phenolic substrates in a microwave radiation field in the presence of TiO_2 particles under UV irradiation," *Environmental Science and Technology*, vol. 38, no. 7, pp. 2198–2208, 2004.

[13] P. Klan, J. Literak, and M. Hajek, "The electrodeless discharge lamp: a prospective tool for photochemistry," *Journal of Photochemistry and Photobiology A*, vol. 128, pp. 145–149, 1999.

[14] L.-Y. Xia, D.-H. Gu, J. Tan, W.-B. Dong, and H.-Q. Hou, "Photolysis of low concentration H_2S under UV/VUV irradiation emitted from microwave discharge electrodeless lamps," *Chemosphere*, vol. 71, no. 9, pp. 1774–1780, 2008.

[15] J. Xu, C. Li, P. Liu, D. He, J. Wang, and Q. Zhang, "Photolysis of low concentration H_2S under UV/VUV irradiation emitted from high frequency discharge electrodeless lamps," *Chemosphere*, vol. 109, pp. 202–207, 2014.

[16] P. M. Álvarez, J. P. Pocostales, and F. J. Beltrán, "Granular activated carbon promoted ozonation of a food-processing secondary effluent," *Journal of Hazardous Materials*, vol. 185, no. 2-3, pp. 776–783, 2011.

[17] J. Jeong, K. Sekiguchi, and K. Sakamoto, "Photochemical and photocatalytic degradation of gaseous toluene using short-wavelength UV irradiation with TiO_2 catalyst: comparison of three UV sources," *Chemosphere*, vol. 57, no. 7, pp. 663–671, 2004.

[18] K.-P. Yu and G. W. M. Lee, "Decomposition of gas-phase toluene by the combination of ozone and photocatalytic oxidation process (TiO_2/UV, TiO_2/UV/O_3, and UV/O_3)," *Applied Catalysis B: Environmental*, vol. 75, no. 1-2, pp. 29–38, 2007.

[19] P. Müller, P. Klán, and V. Ćrkva, "The electrodeless discharge lamp: A prospective tool for photochemistry Part 4: temperature- and envelope material-dependent emission characteristics," *Journal of Photochemistry and Photobiology A: Chemistry*, vol. 158, no. 1, pp. 1–5, 2003.

[20] E. J. Hart, K. Sehested, and J. Holcman, "Molar absorptivities of ultraviolet and visible bands of ozone in aqueous solutions," *Analytical Chemistry*, vol. 55, no. 1, pp. 46–49, 1983.

[21] H. Einaga and S. Futamura, "Catalytic oxidation of benzene with ozone over alumina-supported manganese oxides," *Journal of Catalysis*, vol. 227, no. 2, pp. 304–312, 2004.

[22] H. Huang and W. Li, "Destruction of toluene by ozone-enhanced photocatalysis: performance and mechanism," *Applied Catalysis B: Environmental*, vol. 102, no. 3-4, pp. 449–453, 2011.

[23] B. Liu, A. Li, M. Xia, and Z. Zhu, "Preparation of manganese oxide supported on activated carbon and its application in catalytic ozonation of 4-chlorophenol," *Advanced Materials Research*, vol. 538–541, pp. 2285–2288, 2012.

[24] J. Hoigne and H. Bader, "Rate constants of reactions of ozone with organic and inorganic compounds in water, 1. Non-dissociating organic compounds," *Water Research*, vol. 17, no. 2, pp. 173–183, 1983.

[25] L. M. Dorfman, I. A. Taub, and D. A. Harter, "Rate constants for the reaction of the hydroxyl radical with aromatic molecules," *The Journal of Chemical Physics*, vol. 41, no. 9, pp. 2954–2955, 1964.

[26] H. C. Christensen, K. Sehested, and E. J. Hart, "Formation of benzyl radicals by pulse radiolysis of toluene in aqueous solutions," *The Journal of Physical Chemistry*, vol. 77, no. 8, pp. 983–987, 1973.

[27] J. Ma and N. J. D. Graham, "Degradation of atrazine by manganese-catalysed ozonation: influence of humic substances," *Water Research*, vol. 33, no. 3, pp. 785–793, 1999.

[28] S. Futamura, A. Zhang, H. Einaga, and H. Kabashima, "Involvement of catalyst materials in nonthermal plasma chemical processing of hazardous air pollutants," *Catalysis Today*, vol. 72, no. 3-4, pp. 259–265, 2002.

[29] J. H. Seinfeld and I. Pandis, *Atmospheric Chemistry and Physics: From Air Pollution to Climate Change*, John Wiley & Sons, 2nd edition, 2006.

[30] D. He, A. M. Jones, S. Garg, A. N. Pham, and T. D. Waite, "Silver nanoparticle-reactive oxygen species interactions: application of a charging-discharging model," *Journal of Physical Chemistry C*, vol. 115, no. 13, pp. 5461–5468, 2011.

[31] X. Huang, J. Yuan, J. Shi, and W. Shangguan, "Ozone-assisted photocatalytic oxidation of gaseous acetaldehyde on TiO_2/H-ZSM-5 catalysts," *Journal of Hazardous Materials*, vol. 171, no. 1–3, pp. 827–832, 2009.

[32] M. Kogoma, Y. Miki, K. Tanaka, and K. Takahashi, "Highly efficient VOC decomposition using a complex system (OH radical, ozone-UV, and TiO_2)," *Plasma Processes and Polymers*, vol. 3, no. 9, pp. 727–733, 2006.

[33] M. Sleiman, P. Conchon, C. Ferronato, and J. M. Chovelon, "Photocatalytic oxidation of toluene at indoor air levels (ppbv): towards a better assessment of conversion, reaction intermediates and mineralization," *Applied Catalysis B: Environmental*, vol. 86, no. 3-4, pp. 159–165, 2009.

[34] T. J. Frankcombe and S. C. Smith, "OH-initiated oxidation of toluene. 1. Quantum chemistry investigation of the reaction path," *Journal of Physical Chemistry A*, vol. 111, no. 19, pp. 3686–3690, 2007.

[35] T. J. Frankcombe and S. C. Smith, "OH-initiated oxidation of toluene. 2. Master equation simulation of toluene oxide isomerization," *The Journal of Physical Chemistry A*, vol. 111, no. 19, pp. 3691–3696, 2007.